Available online at www.sciencedirect.com

ScienceDirect

Ceramics International 40 (2014) 4989–4993

CERAMICS INTERNATIONAL

www.elsevier.com/locate/ceramint

Short communication

Spinel lithium titanate from brookite nanocrystallites

Xiangdong Meng*, Xiaocen Wang, Yuxue Zhou, Ling Tong, Xianghua Zeng, Xiaobing Chen

College of Physics Science and Technology, Yangzhou University, Yangzhou, Jiangsu 225002, PR China

Received 19 July 2013; accepted 10 August 2013
Available online 16 August 2013

Abstract

Spinel lithium titanate nanoparticles have been synthesized using anatase and brookite nanocrystallites, as precursors. The corresponding products, A- and B-$Li_4Ti_5O_{12}$ nanoparticles, have distinct differences in the optical absorption property, electrochemical performance and photocatalytic activity. The UV–vis absorption spectrum of B-$Li_4Ti_5O_{12}$ nanoparticles shows strong and wide absorption in the ultraviolet and visible region. B-$Li_4Ti_5O_{12}$ nanoparticles from brookite exhibit a higher discharge capacity than A-$Li_4Ti_5O_{12}$ from anatase. The charge–discharge cycle stability for two types of $Li_4Ti_5O_{12}$ nanoparticles is excellent. Besides, B-$Li_4Ti_5O_{12}$ nanoparticles have much higher photocatalytic activity in the degradation of pollutant $CHCl_3$ than A-$Li_4Ti_5O_{12}$.

Keywords: A. Powders: chemical preparation; B. X-ray methods; D. $Li_4Ti_5O_{12}$; E. Batteries

1. Introduction

Recently, there has been a great deal of interest in spinel $Li_4Ti_5O_{12}$ mainly because of its potential application as electrode material for rechargeable lithium-ion batteries [1–6]. Spinel $Li_4Ti_5O_{12}$ with a theoretical capacity of 175 $mAhg^{-1}$ has a stable charge and discharge plateau at 1.5 V versus Li/Li^+, which could avoid the formation of passive films from the reduction of electrolytes and make batteries safer. The slight change of less than 0.1% in the cell volume during lithium intercalation and de-intercalation results in a long cycling life [7]. Spinel $Li_4Ti_5O_{12}$ was usually prepared by the solid state reaction of TiO_2 and inorganic salt of lithium [2]. The spherical $Li_4Ti_5O_{12}$ was also obtained by hydrothermal synthesis [8]. Anatase or rutile titania was usually used as a starting material in the previous reports [1], but brookite was never used because of the difficulty to prepare pure brookite. The differences in the outcome of solid-state reactions using the different phases of a particular starting material are of great interest for the materials science community. In this work, spinel lithium titanate nanoparticles derived from brookite and anatase nanocrystallites were synthesized, and the effects of titania crystal structure on the properties of $Li_4Ti_5O_{12}$ nanoparticles were investigated.

2. Experimental

All reagents were analytical grade and used without further purification. TiO_2 powder in the pure anatase and brookite phases was respectively prepared using the methods reported in our previous work [9]. The average grain size of anatase and brookite TiO_2 was 10 nm and 150 nm, respectively. In a typical synthesis, 1 g TiO_2 powder in the pure anatase or brookite phase was mixed with 50 ml of 2 M $LiOH \cdot H_2O$ aqueous solution. The resulting suspension was stirred for 10 min and then transferred into stainless autoclave, and held at 200 °C for more than 2 days. The powder products were obtained by carefully filtering and washing the precipitates with deionized water. So-obtainted powder was then annealed at 700 °C for 3 h in atmospheric ambient.

Powder x-ray diffraction (XRD) was performed on a Philips X'Pert Pro Super X-ray diffractometer using CuK_α radiation in an angular range 10°–100° with a 0.01° step width. The size and morphology of lithium titanate nanoparticles were measured by using a Hitachi H-800 transmission electron microscope (TEM, 200 KV). The chemical compositions of two samples were determined with inductively coupled plasma and atomic absorption spectrum (ICP-AAS). The UV–Visible absorption spectra

*Corresponding author. Tel.: +86 514 87991067.
E-mail address: mengxd@yzu.edu.cn (X. Meng).

0272-8842/$ - see front matter © 2013 Elsevier Ltd and Techna Group S.r.l. All rights reserved.
http://dx.doi.org/10.1016/j.ceramint.2013.08.054

(Himadzu, UV-2401) were measured with ethanol as the reference. X-ray photoelectron spectra (XPS) were recorded on a Thermo-VG Escalab 250 X-ray photoelectron spectrometer.

Electrochemical measurements were carried out in a CR2032-type coin cell with lithium metal as the counter electrode. The working electrode was prepared by casting a slurry containing the active material (84 wt%), acetylene black (8 wt%) and poly (vinylidene fluoride) (PVDF) (8 wt%) onto a piece of copper foil. The coin cells were assembled in an argon-filled glove box with 1 M $LiPF_6$ in ethylene carbonate (EC) and diethyl carbonate (DEC) (1:1, v/v) as the electrolyte. The discharge–charge cycling was galvanostatically performed in the voltage range of 0.8–2.7 V at the current rate of 1 C on a battery test instrument (Neware BTS 2300, Shenzhen) at room temperature. The photodegradation reaction of pollutant $CHCl_3$ under visible irradiation from a 120 W metal halide lamp was employed to estimate the photocatalytic activity of lithium titanate nanoparticles. A chloride ion selective electrode was used to measure the Cl^- concentration in the aqueous solution containing $CHCl_3$ and photocatalyst powder and then one could determine the degradation yield.

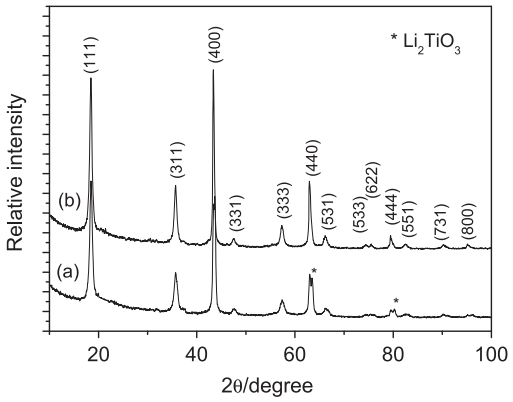

Fig. 1. XRD patterns of lithium titanate: (a) A-$Li_4Ti_5O_{12}$ from anatase and (b) B-$Li_4Ti_5O_{12}$ from brookite.

3. Results and discussion

Fig. 1 shows the XRD patterns of two samples derived from anatase and brookite nanocrystallites, which can be indexed to the same face-centered cubic spinel $Li_4Ti_5O_{12}$ phase (space group $Fd\bar{3}m$, JCPDS no. 49-0207). The element analyses of two samples, performed by ICP-AAS, indicate that the molar ratio of Li/Ti is close to 4:5, consistent with $Li_4Ti_5O_{12}$. In Fig. 1, the diffraction peaks of $Li_4Ti_5O_{12}$ obtained from anatase TiO_2 (labeled hereafter A-$Li_4Ti_5O_{12}$) are basically similar to those of $Li_4Ti_5O_{12}$ obtained from brookite TiO_2 (labeled hereafter B-$Li_4Ti_5O_{12}$). No impurity phases are detected in B-$Li_4Ti_5O_{12}$ and broad nature of the diffraction peaks reveals nanocrystalline nature of spinel $Li_4Ti_5O_{12}$ powder. However, two splitting peaks at $2\theta = 63.5^\circ$ and 80.4°, respectively, imply the presence of a small amount of Li_2TiO_3 impurity in A-$Li_4Ti_5O_{12}$ powder. The size and morphology of $Li_4Ti_5O_{12}$ products were examined by TEM. Fig. 2(a) and (b) are TEM images of the two samples showing that the products consist of nanoparticles. The average grain size of A- and B-$Li_4Ti_5O_{12}$ is 35 nm and 110 nm, respectively.

Appling Rietveld structural refinement, the main structural and compositional parameters are in good agreement with the cation distribution of $(Li)^{8a}[Li_{1/3}Ti_{5/3}]^{16d}O_4^{32e}$. The lattice parameters (a) for A- and B-$Li_4Ti_5O_{12}$ are evaluated to be 8.347 and 8.356 Å, respectively, in accordance with the reported values [7]. The calculated tetrahedra Li3O bond lengths are 1.981 and 1.983 Å for A- and B-$Li_4Ti_5O_{12}$, respectively. It is clear that the difference in the tetrahedra bond length is negligible. However, the calculated octahedra Ti/Li3O bond lengths are 1.994 and 1.978 Å for A- and B-$Li_4Ti_5O_{12}$, respectively, which produces noticeable difference. There are six types of different Ti3O bonds ranging from 1.87 to 2.04 Å in brookite TiO_2 while there are only

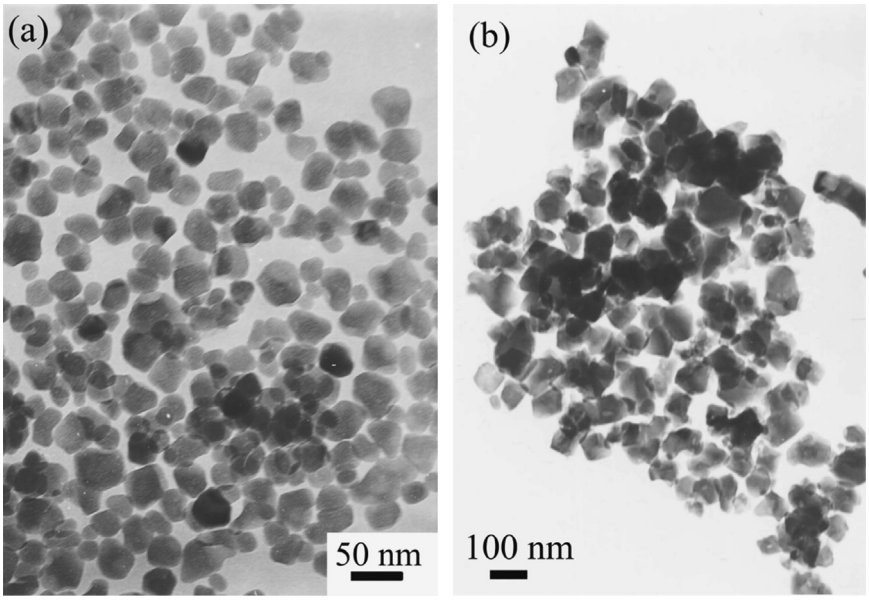

Fig. 2. TEM images of lithium titanate nanoparticles: (a) A-$Li_4Ti_5O_{12}$ and (b) B-$Li_4Ti_5O_{12}$.

two kinds of Ti3O bonds (1.937 and 1.965 Å) in anatase TiO_2 [10], which is the essential difference between brookite and anatase. The transformation from TiO_2 to $Li_4Ti_5O_{12}$ involves the rearrangement of the TiO_6 octahedra units. When the starting brookite TiO_2 is treated with $LiOH \cdot H_2O$ aqueous solution, Li^+ is inserted into the space between TiO_6 octahedra with some of the short Ti3O bonds broken. Thus, it is understandable that the octahedra bond length in B-$Li_4Ti_5O_{12}$ is slightly less than A-$Li_4Ti_5O_{12}$, indicating an increased lattice distortion.

The spinel structure of two samples can be further confirmed by the results of Raman spectra plotted in Fig. 3. The three main bands around 235, 418 and 684 cm^{-1} characteristic of the spinel structure can be ascribed to F_{2u}, E_g and A_{1g} modes, respectively [11,12]. A weak peak at about 328 cm^{-1} present only in Fig. 3b can be also assigned to F_{2u} mode [13,14].

The XPS of Ti (2p) and O (1S) of B-$Li_4Ti_5O_{12}$ are shown in Fig. 4(a) and (b), respectively. The XPS studies of A-$Li_4Ti_5O_{12}$ reveal the similar result which is not presented here. The binding energies at 458.0 and 463.8 eV correspond to the $Ti2p^{3/2}$ and $Ti2p^{1/2}$ of Ti(IV), respectively. Fig. 4(b) shows O (1S) spectra fitted with Gussian distribution. The peaks at 531.5 and 533.0 eV can be ascribed to –OH and H_2O, respectively, while the binding energy at 529.5 eV is attributed to Ti–O in which the valence of Ti is +4 [15]. The surface composition is found to be Li:Ti=4:5 by measuring the area of the Li_{1s} and Ti_{2p} peaks, in agreement with the results of XRD and ICP-AAS.

Fig. 5 shows the UV–visible absorption spectra of A- and B-$Li_4Ti_5O_{12}$ nanoparticles which are ultrasonically dispersed in ethanol. The λ_{onset} of the spectrum recorded from the A-$Li_4Ti_5O_{12}$ nanoparticles is about 340 nm corresponding to a band gap of 3.65 eV. Compared with A-$Li_4Ti_5O_{12}$, the spectrum of B-$Li_4Ti_5O_{12}$ nanoparticles exhibits strong and wide absorption in the ultraviolet and visible region, which can be due to the nonuniformity of defects and size distribution of B-$Li_4Ti_5O_{12}$ nanoparticles. The line broadening of absorption band in the ultraviolet region is associated with the dispersion of nanoparticles and vibrational coupling [16].

Electrochemical performance for two types of $Li_4Ti_5O_{12}$ is investigated in a CR2032-type coin cell at the same rate of 1 C. Fig. 6 shows the initial discharge curves of A- and B-$Li_4Ti_5O_{12}$. It is clear that B- $Li_4Ti_5O_{12}$ derived from brookite has better performance than A-$Li_4Ti_5O_{12}$ from anatase. The discharge capacity of B-$Li_4Ti_5O_{12}$ reaches 163.0 mAh/g, which is close to the theoretical capacity of spinel $Li_4Ti_5O_{12}$. In contrast, A-$Li_4Ti_5O_{12}$ exhibits a lower discharge capacity of 134.2 mAh/g. It can be also seen from Fig. 6 that there exists a flat discharge plateau at 1.5 V which is an intrinsic electrochemical property of spinel $Li_4Ti_5O_{12}$. The capacity of flat voltage can be employed to indicate the mechanism of Li intercalation and de-intercalation. The platform capacity of B-$Li_4Ti_5O_{12}$ is obviously higher than that of A-$Li_4Ti_5O_{12}$. It could be due to the fact that the larger lattice parameter of B- $Li_4Ti_5O_{12}$ comparing to A- $Li_4Ti_5O_{12}$ makes Li^+

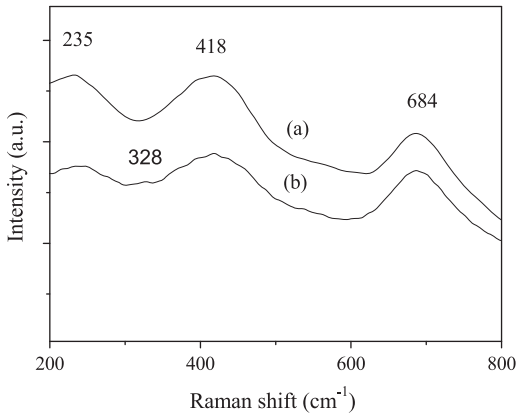

Fig. 3. Raman spectra of lithium titanate nanoparticles: (a) A-$Li_4Ti_5O_{12}$ and (b) B-$Li_4Ti_5O_{12}$.

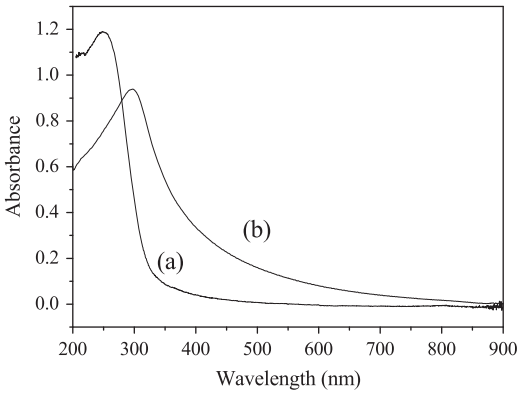

Fig. 5. UV–vis absorption spectra of lithium titanate nanoparticles: (a) A-$Li_4Ti_5O_{12}$ and (b) B-$Li_4Ti_5O_{12}$.

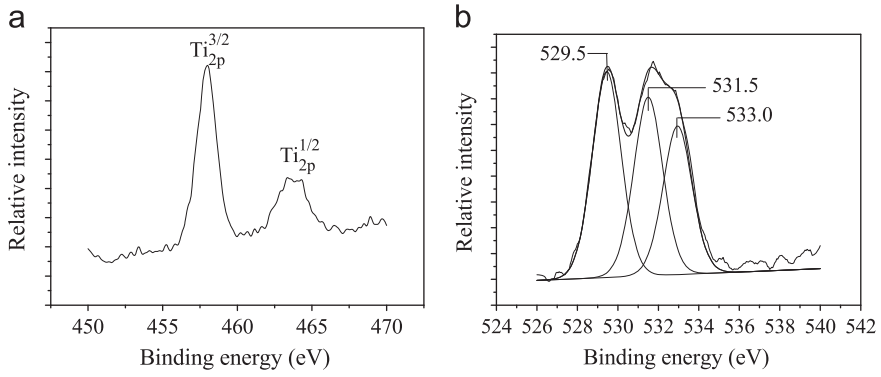

Fig. 4. XP spectra of (a) Ti(2p) and (b) O(1s) of B-$Li_4Ti_5O_{12}$ nanoparticles.

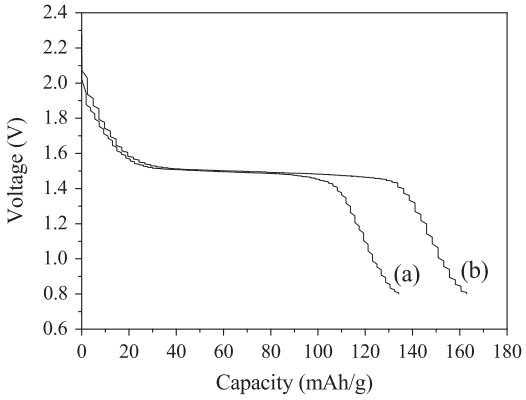

Fig. 6. Initial discharge curves of lithium titanate nanoparticles at 1 C rate: (a) A-$Li_4Ti_5O_{12}$ and (b) B-$Li_4Ti_5O_{12}$.

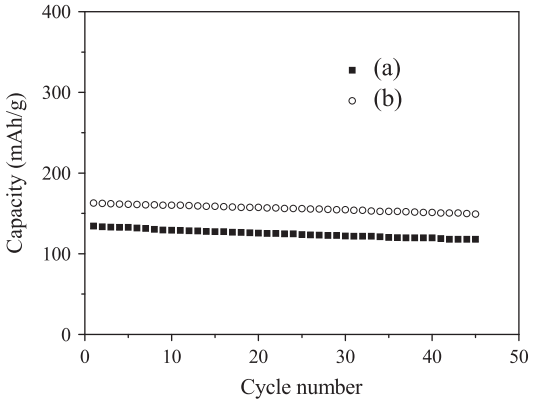

Fig. 7. Cycle life performance of lithium titanate nanoparticles at 1 C rate: (a) A-$Li_4Ti_5O_{12}$ and (b) B-$Li_4Ti_5O_{12}$.

insertion and extraction easier during the charge–discharge process. Furthermore, the higher crystallinity of B-$Li_4Ti_5O_{12}$ with larger grain size can retain the structure integrity during the Li^+ intercalation/deintercalation process and promote the lithium ions diffusion [6]. The higher proportion of platform capacity in the overall capacity is of great significance in the practical application, which also suggests the promising application for B-$Li_4Ti_5O_{12}$ from brookite. Two types of $Li_4Ti_5O_{12}$ exhibit stable cycling performance as shown in Fig. 7. The initial reversible specific capacities of A- and B-$Li_4Ti_5O_{12}$ are 134.2 and 163.0 $mAhg-1$, respectively. After 45 cycles, the capacity value of B-$Li_4Ti_5O_{12}$ decreases to 143.9 $mAhg-1$ with a capacity loss of 0.18% per cycle, while the capacity of A-$Li_4Ti_5O_{12}$ retains 117.9 $mAhg-1$ at 45th cycle with a capacity loss of 0.27% per cycle.

The photocatalytic activity of A- and B-$Li_4Ti_5O_{12}$ for degradation of $CHCl_3$ under visible irradiation is shown in Fig. 8. Pollutant $CHCl_3$ can be photocatalytically decomposed into CO_2 and HCl in the liquid phase following the process:

$$CHCl_3 + H_2O + 0.5O_2 \rightarrow CO_2 + 3HCl.$$

The photocatalytic activity of B-$Li_4Ti_5O_{12}$ is much higher than that of A-$Li_4Ti_5O_{12}$ for the same degradation compound. The degradation percentage of $CHCl_3$ on B-$Li_4Ti_5O_{12}$ nanoparticles reaches almost 100% after the visible irradiation of

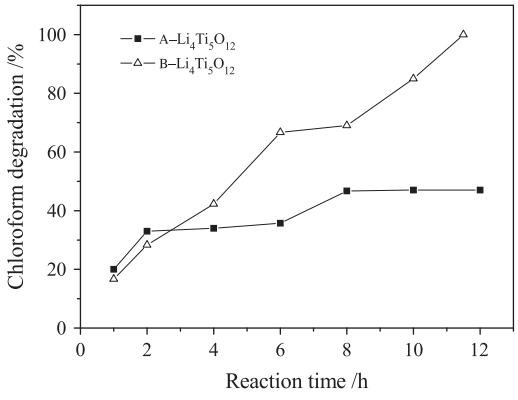

Fig. 8. Degradation of chloroform ($CHCl_3$) on lithium titanate nanoparticles.

12 h, in comparison with the degradation percentage of 47% for A-$Li_4Ti_5O_{12}$. Considering that B-$Li_4Ti_5O_{12}$ has a strong and wide absorption in the visible region as mentioned above, the excellent photocatalytic activity of B-$Li_4Ti_5O_{12}$ can be easily understood. B-$Li_4Ti_5O_{12}$ can produce more photogenerated electrons and holes under visible irradiation than A-$Li_4Ti_5O_{12}$. In addition, hydroxyl absorbed on the surface of B-$Li_4Ti_5O_{12}$ can combine with the surface-trapped hole to produce $^{\bullet}OH$ radical that acts strong oxidation activity [17], which can make contribution to enhance the photocatalytic activity of B-$Li_4Ti_5O_{12}$.

4. Conclusions

A- and B-$Li_4Ti_5O_{12}$ nanoparticles with spinel structure have been synthesized by using anatase and brookite nanocrystallites, respectively, as precursors. The differences between A- and B-$Li_4Ti_5O_{12}$ in properties are investigated. B-$Li_4Ti_5O_{12}$ nanoparticles exhibit strong and wide absorption in both ultraviolet and visible region, which is in favor of the enhancement of photocatalytic activity of B-$Li_4Ti_5O_{12}$ under visible irradiation. B-$Li_4Ti_5O_{12}$ derived from brookite has better electrochemical performance than A-$Li_4Ti_5O_{12}$ from anatase, which can be associaded with the larger lattice parameter and the higher crystallinity of B-$Li_4Ti_5O_{12}$. The discharge capacity of B-$Li_4Ti_5O_{12}$ reaches 163.0 mAh/g at 1 C with a higher proportion of platform capacity and fairly stable cycling performance.

Acknowledgment

This work is supported by the National Natural Science Foundation of China (Grant no. 21101135).

References

[1] T. Yuan, R. Cai, P. Gu, Z.P. Shao, Synthesis of lithium insertion material $Li_4Ti_5O_{12}$ from rutile TiO_2 via surface activation, Journal of Power Sources 195 (2010) 2883–2887.

[2] Y.L. Qia, Y.D. Huang, D.Z. Jia, S.J. Bao, Z.P. Guo, Preparation and characterization of novel spinel $Li_4Ti_5O_{12-x}Br_x$ anode materials, Electrochimica Acta 54 (2009) 4772–4776.

[3] T. Yuan, R. Cai, K. Wang, R. Ran, S.M. Liu, Z.P. Shao, Combustion synthesis of high-performance $Li_4Ti_5O_{12}$ for secondary Li-ion battery, Ceramics International 35 (2009) 1757–1768.
[4] X.F. Guo, C.Y. Wang, M.M. Chen, A novel non-organic hydrothermal/hydrolysis method for preparation of well-dispersed $Li_4Ti_5O_{12}$, Materials Letters 83 (2012) 39–41.
[5] J.J. Huang, Z.Y. Jian, The preparation and characterization of $Li_4Ti_5O_{12}$/carbon nano-tubes for lithium ion battery, Electrochimica Acta 53 (2008) 7756–7759.
[6] N.Q. Zhang, Z.M. Liu, T.Y. Yang, C.L Liao, Z.J. Wang, K.N. Sun, Facile preparation of nanocrystalline $Li_4Ti_5O_{12}$ and its high electrochemical performance as anode material for lithium-ion batteries, Electrochemistry Communications 13 (2011) 654–656.
[7] T. Ohzuku, A. Ueda, N. Yamamoto, Zero-strain insertion material of Li $[Li_{1/3}Ti_{5/3}]O_4$ for rechargeable lithium cells, Journal of the Electrochemical Society 142 (1995) 1431–1435.
[8] Z.W. Zhang, L.Y. Cao, J.F. Huang, D.Q. Wang, J.P. Wu, Y.J. Cai, Hydrothermal synthesis of $Li_4Ti_5O_{12}$ microsphere with high capacity as anode material for lithium ion batteries, Ceramics International 39 (2013) 2695–2698.
[9] X.D. Meng, D.Z. Wang, J.H. Liu, S.Y. Zhang, Preparation and characterization of sodium titanate nanowires from brookite nanocrystallites, Materials Research Bulletin (2004) 2163–2170.
[10] S.D. Mo, W.Y. Ching, Electronic and optical properties of three phases of titanium dioxide: rutile, anatase, and brookite, Physical Review B 51 (1995) 13023–13032.
[11] L. Aldon, P. Kubiak, M. Womes, J.C. Jumas, J. Olivier-Fourcade, J.L. Tirado, J.I. Corredor, C. Perez Vicente, Chemical and electrochemical Li-insertion into the $Li_4Ti_5O_{12}$ spinel, Chemistry of Materials 16 (2004) 5721–5725.
[12] Y. Qiao, X.L. Hu, Y. Liu, Y.H. Huang, $Li_4Ti_5O_{12}$ nanocrystallites for high-rate lithium-ion batteries synthesized by a rapid microwave-assisted solid-state process, Electrochimica Acta 63 (2012) 118–123.
[13] D. Capsoni, M. Bini, V. Massarotti, P. Mustarelli, S. Ferrari, G. Chiodelli, M.C. Mozzati, P. Galinetto, Cr and Ni doping of $Li_4Ti_5O_{12}$: cation distribution and functional properties, the Journal of Physical Chemistry C 113 (2009) 19664–19671.
[14] S.L. Chou, J.Z. Wang, H.K. Liu, S.X. Dou, Rapid synthesis of $Li_4Ti_5O_{12}$ microspheres as anode materials and its binder effect for lithium-ion battery, the Journal of Physical Chemistry C 115 (2011) 16220–16227.
[15] ⟨http:/srdata.nist.gov/xps⟩.
[16] T. Trindade, P. O'Brien, X.M. Zhang, Synthesis of CdS and CdSe nanocrystallites using a novel single-molecule precursors approach, Chemistry of Materials 9 (1997) 523–530.
[17] A.L. Linsebigler, G. Lu, T.Y. John, Photocatalysis on TiO_2 surfaces: principles, mechanisms, and selected results, Chemical Reviews 95 (1995) 735–758.